Abstracta

Ano XXVII - N. 03

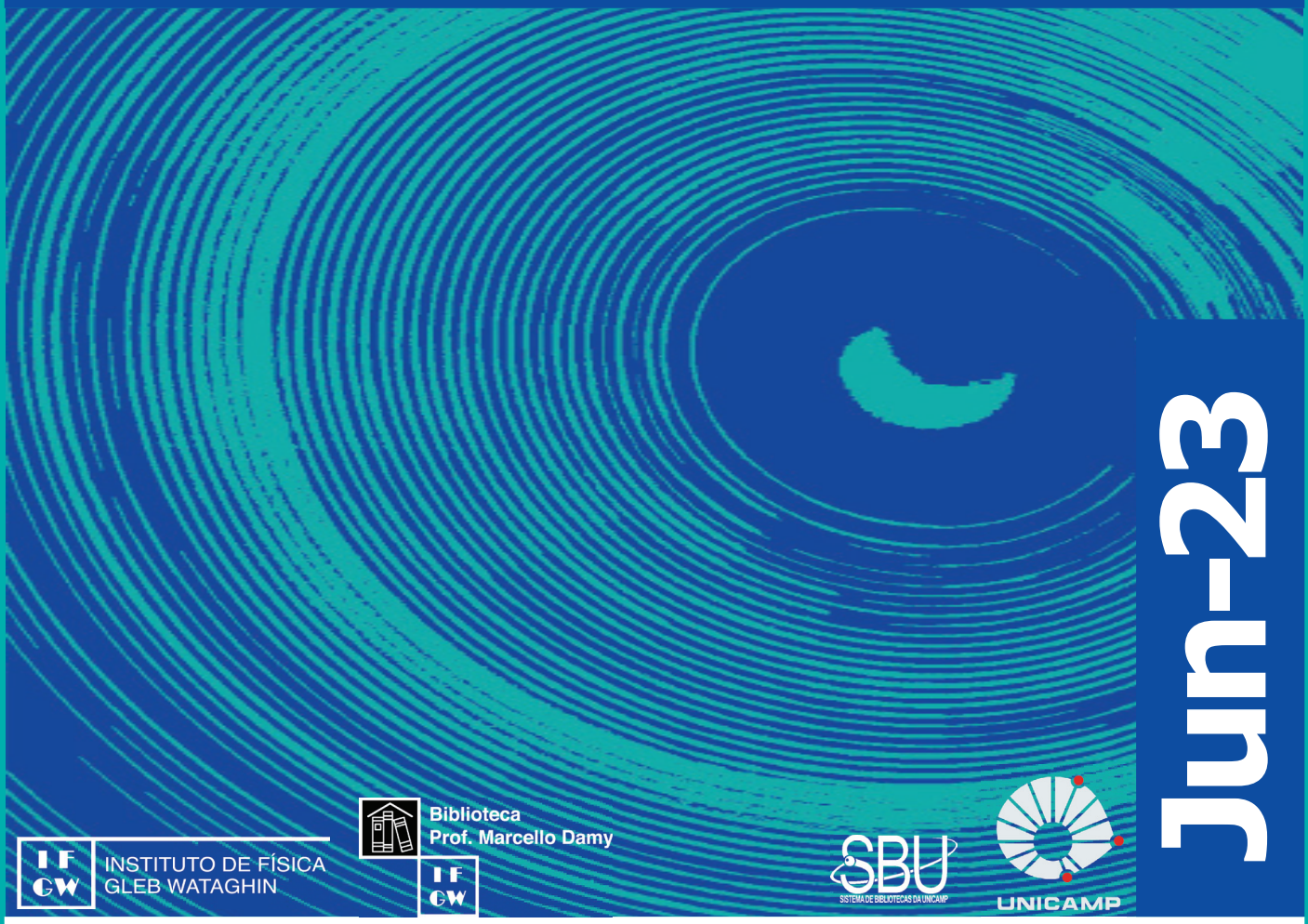

Artigos publicados - P041-2023 à P102-2023

Defesas de Dissertações do IFGW - D005-2023 à D010-2023

Defesas de Teses do IFGW - T004-2023 à T008-2023

Defesas de Dissertações e Teses do PECIM - Pe001-2023

Artigos publicados

[P041-2023] "A reappraisal of the principle of equivalent time based on physicochemical methods"

Rufino, M.*; Lixandrao, A. L.*; Guedes, S.*

The main feature of the Fission-Track Thermochronology is its ability to infer the thermal histories of mineral samples in regions of interest for geological studies. The ingredients that make the thermal history inference possible are the annealing models, which capture the annealing kinetics of fission tracks for isothermal heating experiments, and the Principle of Equivalent Time (PET), which allows the application of the annealing models to variable temperatures. It turns out that the PET only applies to specific types of annealing models describing single activation energy annealing mechanisms (parallel models). However, the PET has been extensively applied to models related to multiple activation energy mechanisms (fanning models). This procedure is an approxi-mation that has been overlooked due to the lack of a suitable alternative. To deal with this difficult, a formalism, based on physicochemical techniques, that allows to quantify the effects of annealing on the fission tracks for variable temperatures, is developed. It is independent of the annealing mechanism and, therefore, is applicable to any annealing model. In the cases in which the PET is valid, parallel models, the proposed method and the PET predict the same degrees of annealing. However, deviations appear when the methods are applied to the fanning models, with the PET underestimating annealing effects. The consequences for the inference of thermal histories are discussed.

CHEMICAL GEOLOGY 627, 121459, 2023. DOI: 10.1016/j.chemgeo.2023.121459

[P042-2023] "A Rodent Model of Human-Dose-Equivalent 5-Fluorouracil: Toxicity in the Liver, Kidneys, and Lungs"

Silva, M. C. da; Fabiano, L. C.; Salomao, K. C. da C.; Freitas, P. L. Z. de; Neves, C. Q.; Borges, S. C.; Carvalho, M. das. G. de S.; Breithaupt-Faloppa, A. C.; **Thomaz, A. A. de***; Santos, A. M. dos; Buttow, N. C.

5-Fluorouracil (5-FU) is a chemotherapy drug widely used to treat a range of cancer types, despite the recurrence of adverse reactions. Therefore, information on its side effects when administered at a clinically recommended dose is relevant. On this basis, we examined the effects of the 5-FU clinical treatment on the integrity of the liver, kidneys, and lungs of rats. For this purpose, 14 male Wistar rats were divided into treated and control groups and 5-FU was administered at 15 mg/kg (4 consecutive days), 6 mg/kg (4 alternate days), and 15 mg/kg on the 14th day. On the 15th day, blood, liver, kidney, and lung samples were collected for histological, oxidative stress, and inflammatory evaluations. We observed a reduction in the antioxidant markers and an increase in lipid hydroperoxides (LOOH) in the liver of treated animals. We also detected elevated levels of inflammatory markers, histological lesions, apoptotic cells, and aspartate aminotransferase. Clinical treatment with 5-FU did not promote inflammatory or oxidative alterations in the kidney samples; however, histological and biochemical changes were observed, including increased serum urea and uric acid. 5-FU reduces endogenous antioxidant defenses and increases LOOH levels in the lungs, suggesting oxidative stress. Inflammation and histopathological alterations were also detected. The clinical protocol of 5-FU promotes toxicity in the liver, kidneys, and lungs of healthy rats, resulting in different levels of histological and biochemical alterations. These results will be useful in the search for new adjuvants to attenuate the adverse effects of 5-FU in such organs.

ANTIOXIDANTS 125[5], 1005, 2023. DOI: 10.3390/antiox12051005

[P043-2023] "A simple and precise way to determine electrical resistivity of isotropic conductors: Simplifying the four-probe method"

Alves, L. M. S.; **Oliveira, F. S.***; Romao, E. C.; Luz, M. S. da; Santos, C. A. M. dos

Numerical simulations via COMSOL Multiphysics software are used to describe the behavior of electrical resistivity of several samples with rectangular shape typically used in the Montgomery method. The simulation data obtained using four isotropic conductors allowed us to understand in detail the behavior of the electric potential and electric field of the samples. The results provide an analytical method, which can substitute the four-probe method with much more simplicity and precision.

AIP ADVANCES 13[3], 035134, 2023. DOI: 10.1063/5.0139613

[P044-2023] "Addressing the Magnitude of the Nonlinear Refraction Response in Perovskite Nanocrystals"

Sousa, C. A.*; Bonato, L. G.*; Goncalves, E. S.*; Alo, A.*; Vale, B. R. C.*; Almeida, D. B.*; Nogueira, A. F.; **Zagonel, L. F.*; Padilha, L. A.***

Colloidal perovskite nanocrystals (PNCs) are among the most studied optical materials in the last decade. Because of their remarkable optical properties, such as high photoluminescence quantum yield, narrow emission spectra, and high tunability in the visible range, they have become important candidates for several applications in optoelectronics technologies. Most recently, several reports have claimed that this class of nanomaterials also possesses outstanding third-order nonlinear optical properties, such as a high two-photon absorption cross section and a high nonlinear refractive index. In this paper, we investigate the nonlinear optical response for a series of CsPbBr3 PNCs and show that their nonlinear optical response is not particularly high. Different from what has been claimed in the literature, we show that no evidence is found to support that the nonlinear refractive index for these PNCs is larger than those observed for other semiconductors, as the measured magnitude varies between 10-14 and 10-13 cm2/W, the same order of magnitude as bulk semiconductors with a similar band gap energy.

ACS PHOTONICS, 2023. DOI: 10.1021/acsphotonics.2c01985
Primeira data de acesso: APR 2023

[P045-2023] "Application of a new lignin/cellulose carbon xerogel/ZnO/Bi2O3/Bi degrees composite photocatalyst for the degradation of bisphenol-A under sunlight"

Moraes, N. P. de; Campos, T. M. B.; Thim, G. P.; **Siervo, A. de***; Lanza, M. R. de V.; Rodrigues, L. A.

This work proposed the study of a new lignin/cellulose carbon xerogel/ZnO/Bi2O3/Bi degrees composite photocatalyst for the degradation of bisphenol-A under sunlight. The reasoning behind the application of each component is based on the formation of multiple heterojunctions (p-n heterojunction between semiconductors, metal-semiconductor heterojunction, and carbon-semiconductor heterojunction) to hinder the recombination of pho-togenerated charges during the photocatalytic process. The lignin/cellulose carbon xerogel was employed as both a solid electron mediator and a reducing agent, promoting the reduction of the bismuth oxide into metallic bismuth. The results obtained from the characterization tests confirm the formation of all the intended phases in the hybrid photocatalyst. Furthermore, the inclusion of the carbon xerogel led to morphological modifications such as the formation of plate-like particles and the increase of specific surface area.

The efficient formation of the heterojunctions between the composing phases of the hybrid composite led to an enhanced photocatalytic activity for the degradation of the bisphenol-A (BPA) molecule, under both simulated sunlight and visible light. The optimized composite achieved 84% degradation of the BPA under simulated sunlight and 27% under visible light irradiation, which is a great improvement in comparison to the pure ZnO, which obtained 55% degradation under simulated sunlight and 19% degradation under visible light. The enhanced photocatalytic activity of the lignin/cellulose carbon xerogel/ZnO/Bi2O3/Bi degrees composite was further verified by chronoamperometry tests, which evidenced its greater photocurrent generation capabilities.

CHEMICAL PHYSICS IMPACT 6, 100182, 2023. DOI: 10.1016/j.chphi.2023.100182

[P046-2023] "Assessing the ultracentral flow puzzle in hydrodynamic modeling of heavy-ion collisions"

Giannini, A. V.*; Ferreira, M. N.*; Hippert, M.; **Chinellato, D. D.***; Denicol, G. S.; Luzum, M.; Noronha, J.; Silva, T. N. da; **Takahashi, J.***

An outstanding problem in heavy-ion collisions is the inability for models to accurately describe ultracentral experimental flow data, despite that being precisely the regime where a hydrodynamic description should be most applicable. We reassess the status of this puzzle by computing the flow in ultracentral collisions obtained from multiple recent Bayesian models that were tuned to various observables in different collision systems at typical centralities. While central data can now be described with better accuracy than in previous calculations, tension with experimental observation remains and worsens as one goes to ultracentral collisions. Tuning the model parameters cannot remove this tension without destroying the fit at other centralities. As such, new elements are likely needed in the standard modeling of heavy-ion collisions.

PHYSICAL REVIEW C 107[4], 044907, 2023. DOI: 10.1103/PhysRevC.107.044907

[P047-2023] "Boron nitride nanotube peapods at ultrasonic velocity impacts: a fully atomistic molecular dynamics investigation"

Sousa, J. M. de*; Machado, L. D.; Woellner, C. F.; Medina, M.; Autreto, P. A. S.; **Galvao, D. S.***

Boron nitride nanotube peapods (BNNT-peapod) are composed of linear chains of C-60 molecules encapsulated inside BNNTs, they were first synthesized in 2003. In this work, we investigated the mechanical response and fracture dynamics of BNNT-peapods under ultrasonic velocity impacts (from 1 km s(-1) up to 6 km s(-1)) against a solid target. We carried out fully atomistic reactive molecular dynamics simulations using a reactive force field. We have considered the case of horizontal and vertical shootings. Depending on the velocity values, we observed tube bending, tube fracture, and C-60 ejection. Furthermore, the nanotube unzips for horizontal impacts at certain speeds, forming bi-layer nanoribbons 'incrusted' with C-60 molecules. The methodology used here is applicable to other nanostructures. We hope it motivates other theoretical investigations on the behavior of nanostructures at ultrasonic velocity impacts and aid in interpreting future experimental results. It should be stressed that similar experiments and simulations were carried out on carbon nanotubes trying to obtain nanodiamonds. The present study expands these investigations to include BNNT.

JOURNAL OF PHYSICS-CONDENSED MATTER 35[33], 335701, 2023. DOI: 10.1088/1361-648X/acd50b

[P048-2023] "Boroxine benzaldehyde complex for pharmaceutical applications probed by electron interactions"

Pereira-da-Silva, J.; Nunes, A.; Mendes, M.; Rodrigues, R.; **Cornetta, L.***; Silva, F. F. da

Rationale 2,4,6-Tris(4-formylphenyl)boroxine (TFPB) is a substituted boroxine containing a benzaldehyde molecule bonded to each boron atom. Boroxine cages are an emerging class of functional nanostructures used in host-guest chemistry, and benzaldehyde is a potential radiosensitizer. Reactions initiated by low-energy electrons with such complexes may dictate and bring new fundamental knowledge for biomedical and pharmaceutical applications. Methods The electron ionization properties of TFPB are investigated using a gas-phase electron-molecule crossed beam apparatus coupled with a reflectron time-of-flight mass spectrometer in an orthogonal geometry. Ionization and threshold energies are experimentally determined by mass spectra acquisition as a function of the electron energy. Results The abundance of the molecular precursor cation in the mass spectrum at 70 eV is significantly lower than that of the most abundant fragment C7H5O+. Twenty-nine cationic fragments with relative intensities >2% are detected and identified. The appearance energies of six fragment cations are reported, and the experimental first ionization potential is found at 9.46 +/- 0.11 eV. Moreover, eight double cations are identified. The present results are supported by quantum chemical calculations based on bound state techniques, electron ionization models and thermodynamic thresholds. Conclusions According to these results, the TPFB properties may combine the potential radiosensitizer effect of benzaldehyde with the stability of the boroxine ring.

RAPID COMMUNICATIONS IN MASS SPECTROMETRY 37[1], e9418, 2023. DOI: 10.1002/rcm.9418

[P049-2023] "Brain volumes and white matter diffusion across the adult lifespan in temporal lobe epilepsy"

Yasuda, C. L.; Pimentel-Silva, L. R.; **Beltramini, G. C.***; Liu, M.; Campos, B. M. de; Coan, A. C.; Beaulieu, C.; Cendes, F.; Gross, D. W.

Objective: Typical aging is associated with gradual cognitive decline and changes in brain structure. The observation that cognitive performance in mesial temporal lobe epilepsy (TLE) patients diverges from controls early in life with subsequent decline running in parallel would suggest an initial insult but does not support accelerated decline secondary to seizures. Whether TLE patients demonstrate similar trajectories of age-related gray (GM) and white matter (WM) changes as compared to healthy controls remains uncertain. Methods: 3D T1-weighted and diffusion tensor images were acquired at a single site in 170 TLE patients (aged 23-74 years) with MRI signs of unilateral hippocampal sclerosis (HS, 77 right) and 111 healthy controls (aged 26-80 years). Global brain (GM, WM, total brain, and cerebrospinal fluid) and regional volumes (ipsi- and contralateral hippocampi), and fractional anisotropy (FA) of 10 tracts (three portions of corpus callosum, inferior longitudinal, inferior fronto-occipital and uncinate fasciculi, body of fornix, dorsal and parahippocampal-cingulum, and corticospinal tract) were compared between groups as a function of age. Results: There were significant reductions of global brain and hippocampi volumes (greatest ipsilateral to HS), and FA of all 10 tracts in TLE versus controls. For TLE patients, regression lines run in parallel to those from controls for brain volumes and FA (for all tracts except the parahippocampal-cingulum and corticospinal tract) versus age across the adult lifespan. Interpretation: These results imply a developmental hindrance occurring earlier in life (likely in childhood/neurodevelopmental stages) rather than accelerated atrophy/degeneration of most brain structures herein analyzed in patients with TLE.

ANNALS OF CLINICAL AND TRANSLATIONAL NEUROLOGY, 2023. DOI: 10.1002/acn3.51793 Primeira data de acesso: MAY 2023

[P050-2023] "Bulk and surface electronic structure of NiBi3"

Adriano, C.*; Lee, K. Y. C.; Kushnirenko, Y.; Schrunk, B.; **Pakuszewski, K. R.***; Wang, L. L.; Bud'ko, S. L.; Canfield, P. C.; Kaminski, A.

We present a high-resolution, angle-resolved photoemission spectroscopy study of the normal electronic state of the superconducting NiBi3. Our experimental results show a complex Fermi surface structure with many sheets along the P -X and P -Y directions of the Brillouin zone. The band structure presents a topological surface state (TSS) at the high symmetry I' point with a surface Dirac point at the energy -0.185 eV. The Dirac-like cone presents a linear dispersion along kx while it presents saddle-like states along ky located in the vicinity of the surface Dirac point. Our results are in good agreement with results of density functional theory band structure calculations. We also discuss the topological band structure of the NiBi3 compound.

PHYSICAL REVIEW B 107[16], 165107, 2023. DOI: 10.1103/PhysRevB.107.165107

[P051-2023] "Characterization of lipid systems based on fully hydrogenated soybean and high oleic sunflower oils to obtain nanostructured lipid carriers"

Ludtke, F. L.; Stahl, M. A.; Grimaldi, R.; **Cardoso, L. P.***; Ribeiro, A. P. B.

Resistance to chemical degradation, a melting point above body temperature, biodegradability, and generally regarded as safe status are prerequisites for a lipid matrix to produce nanostructured lipid carriers (NLC). This study aimed to evaluate the composition and physical and crystallization properties of lipid systems composed of fully hydrogenated soybean oil (FHSO) and high oleic sunflower oil (HOSO). The lipid systems were charac--terized by their composition in fatty acids and triacylglycerol (TAG), thermal behavior during melting and crystallization, solid fat content (SFC), microscopical features, and polymorphism. Elevated HOSO in lipid sys-tems promoted an increase in unsaturated fatty acids (UFA) and di-and tri-unsaturated TAG, a reduction in SFC and in crystalized areas and variations in thermal behavior. Excepted lipid system 10:90 FHSO:HOSO (w/w), all systems exhibited polymorphic stabilization in beta form after 60 days. Findings of the present study demonstrated that the raw materials are compatible for the formulation of NLC.

FOOD BIOSCIENCE 53, 102634, 2023. DOI: 10.1016/j.fbio.2023.102634

[P052-2023] "Composite magnetic properties of cobalt ferrite nanoparticles embedded in bacterial nanocellulose of different porosity levels"

Menchaca-Nal, S.; Jativa-Herrera, J. A.; Moscoso-Londono, O.; Pampillo, L. G.; Martinez-Garcia, R.; **Knobel, M.***; Londono--Calderon, C. L.

A simple and novel strategy for tuning the macroporous structure of bacterial nanocellulose allows for embed--ding nanoparticles on the template. Here, cobalt ferrite nanoparticles were co-precipitated in-situ at two tem-plates with different porosities. Different analytical techniques like SEM, XRD, TGA, and PPMS allow for characterizing the properties of the prepared magnetic nanocomposites. After eight months of aging at room conditions, lyophilized bacterial nanocellulose preserved the macroporous structure (porosity -46%). However, rehydration and re-lyophilization of the cellulose decrease the template porosity (-8%). The cobalt ferrite nanoparticles, growth on high and low macroporous templates, were single-crystalline and microstrain-free. The nanoparticle's shape and mean size do not change with the porosity of the template, but the cluster size does. However, the differences in porosity on templates allow tuning the nanoparticle concentration and then its magnetic interactions (in high macroporous near 63%, and low about 43%) in the nanocomposites. Magnetic data confirm the influence of the template porosity on the magnetic particle concentration. The magnetic behavior as a temperature function (effective magnetic anisotropy constant, coercive force, and reduced remanence) is dependent on the template porosity. These dissimilarities were correlated with cluster size vari-ations, where the differences in the aggregation modify the magnetic dipolar interactions among particles.

MATERIALS CHEMISTRY AND PHYSICS 303, 127798, 2023. DOI: 10.1016/j.matchemphys.2023.127798

[P053-2023] "Coupled mode theory revisited: the role of the network topology and ordered directionality"

Rezende, G. F. M.*; Kersul, C. M.*; Barea, L. A. M.; Ascengao, G. R.; **Assis, P. L. de*; Frateschi, N. C.***

We propose a theoretical correction to the coupled mode theory (CMT) to describe three or more coupled optical resonators considering the topological placement of each resonator and the light flow direction. This work allows an expansion of the CMT approximation for strong coupling and is validated by employing the transfer matrix method. A model of the three coupled resonators was studied in detail to provide evidence of the significant improvement in predicting the transmission spectrum of dark modes.

JOURNAL OF THE OPTICAL SOCIETY OF AMERICA B-OPTICAL PHYSICS 40[5], 1005-1016, 2023. DOI: 10.1364/JOSAB.482606

[P054-2023] "Crystalline Structure, Morphology, and Adherence of Thick TiO2 Films Grown on 304 and 316L Stainless Steels by Atomic Layer Deposition"

Marques, V. E. C.; Manfroi, L. A.; Vieira, A. A.; Pereira, A. L. de J.; **Marques, F. das C.***; Vieira, L.

Titanium dioxide (TiO2) thin films are widely used in transparent optoelectronic devices due to their excellent properties, as well as in photocatalysis, cosmetics, and many other biomedical applications. In this work, TiO2 thin films were deposited onto AISI 304 and AISI 316L stainless steel substrates by atomic layer deposition, followed by comparative evaluation of the mixture of anatase and rutile phase by X-ray diffraction, Raman maps, morphology by SEM-FEG-AFM, and adhesion of the films on the two substrates, aiming to evaluate the scratch resistance. Raman spectroscopy mapping and X-ray diffraction with Rietveld refinement showed that the films were composed of anatase and rutile phases, in different percentages. Scratch testing using a diamond tip on the TiO2 film was employed to evaluate the film adherence and to determine the friction coefficient, with the results showing satisfactory adherence of the films on both substrates.

COATINGS 13[4], 757, 2023. DOI: 10.3390/coatings13040757

[P055-2023] "Decoupling Chemically Active 2D Molecular Overlayers from the Substrate: Chlorophenyl Porphyrins on Graphene/Ir(111)"

Mowbray, D. J.; Paz, A. P.; Ferreira, R. C. C.; Milotti, V.; Schio, P.; Silva, W. S. E.; Pichler, T.; **Siervo, A. de***; Moreno-Lopez, J. C.

The synthesis of atomically precise chemically active 2D molecular overlayers may be hindered by chemical interactions with the underlying substrate, especially when based on chlorophenyl porphyrins. At the same time, the chlorination of graphene, i.e., the covalent bonding of chlorine atoms with sp2 carbon atoms, is known to have a significant influence on the electronic properties of pristine graphene. In this study, we deposit a chlorinated porphyrin molecule, namely 5,10,15,20-tetrakis(4chlorophenyl)porphyrin (Cl4TPP), on graphene/Ir(111). Employing a combined experimental and theoretical approach, we demonstrate that the porphyrin layer physisorbed on graphene self-assembles into a periodic square-like arrangement. This carpet like growth is unperturbed by the step edges of the substrate, neither in its periodicity nor in its orientation. In addition, the molecular overlayer is thermally stable and does not alter the electronic properties of graphene. Remarkably, we show that Cl4TPP does not experience a dechlorination reaction with the underlying substrate, even after postdeposition annealing temperatures as high as 550 K. Moreover, postdeposition annealing at 700 K suggests the Cl4TPP molecules desorb intact without affecting graphene's electronic properties. In so doing, we demonstrate the effectiveness of graphene physisorbed on Ir(111) to both promote the formation and preserve the properties of chemically reactive 2D overlayers based on chlorophenyl porphyrins. These results show physisorbed graphene's potential as a general templating material for the formation of highly reactive self-assembled 2D overlayers.

JOURNAL OF PHYSICAL CHEMISTRY C 127[18], 8751-8758, 2023. DOI: 10.1021/acs.jpcc.3c00235

[P056-2023] "Desorption of chemical species during thermal reduction of graphene oxide films"

Viana, G. A.*; Silva, D. S. da*; Landers, R.*; Freitas, J. N. de; Villalva, M. G.; **Marques, F. das C.***

Graphene oxide (GO) reduced by thermal or chemical processes has been used in conductive transparent layers, solar cells, chemical sensors among dozens of other applications. Although some researchers have focused on identifying the reduction mechanisms, there is a lack of detailed investigation of species effusion processes. Here we report a systematic investigation on the effusion of chemical species from thermally reduced multilayered GO using the thermal desorption mass spectroscopy technique. The identification of chemical species with the use of the mass spectrometer associated with the formation energy was used to identify the reactions that occur in GO during the thermal reduction. This allows to give support or rule out numerous proposals for effusion processes in GO presented in the literature. It was observed that the main desorption regime centered at similar to 230 degrees C encompassed a collective desorption of H2O, CO2, CO, and H with formation energies ranging from 1.20 to 1.40 eV. For temperatures higher than 400 degrees C, uncoupled CO2 and CO desorptions were the only species detected, with formation energies of 1.87 and 3.09 eV, respectively. An insulating-conductive transition occurred in the annealing temperature range (ambient to 1000 degrees C) with a variation of 7 orders of magnitude in conductivity. The results support new routes for reducing GO in order to obtain films closer to pristine graphene multilayers.

SURFACE & COATINGS TECHNOLOGY 463, 129524, 2023. DOI: 10.1016/j.surfcoat.2023.129524

[P057-2023] "Detection of Surface States in Quantum Materials ZrTe2 and TmB4 by Scanning Tunneling Microscopy"

Crivillero, M. V. A.; **Souza, J. C.***; Hasse, V.; Schmidt, M.; Shitsevalova, N.; Gabani, S.; Siemensmeyer, K.; Flachbart, K.; Wirth, S.

Scanning Tunneling Microscopy and Spectroscopy (STM/S), with its exceptional surface sensitivity and exquisite energy resolution, is well suited for the investigation of surface states down to atomic length scales. As such, it became an essential tool to probe the surface states of materials, including those with non-trivial topology. One challenge, however, can be the preparation of clean surfaces which allow the study of preferably unchanged surface properties with respect to the bulk amount. Here, we report on the STM/S of two materials, ZrTe2 and TmB4. The former cleaves easily and defects can be examined in detail. However, our STS data can only qualitatively be compared to the results of band structure calculations. In the case of TmB4, the preparation of suitable surfaces is highly challenging, and atomically flat surfaces (likely of B-termination) were only encountered rarely. We found a large density of states (DOS) at the Fermi level EF and a mostly featureless differential conductance near EF. Further efforts are required to relate our results to the electronic structure predicted by ab initio calculations.

CONDENSED MATTER 8[1], 9, 2023. DOI: 10.3390/condmat8010009

[P058-2023] "Determination of Co2+ ions in blood samples: A multi-way sensing based on NH2-rich carbon quantum dots"

Oliveira, J. J. P.; Carneiro, S. V.; Cruz, A. A. C.; Fechine, L. M. U. D.; Michea, S.; Antunes, R. A.; **Neto, M. L. A.***; Moura, T. A.; **Cesar, C. L.*; Carvalho, H. F.***; Paschoal, A. R.; Lopes, G. S.; Freire, R. M.; Fechine, P. B. A.

Multiple forms of detecting Co2+ are reported in this work to quantify these ions in real blood plasma samples. Carbon Quantum Dots (CQDs) were used as a fluorescent nanoprobe. The CQDs were obtained from a bottom-up approach using a hydrothermal method and choline chloride and branched poly(ethyleneimine) as precursor molecules. Several spectroscopic and structural characterizations were performed. The efficient fluorescence quenching of CQDs related to the Co2+ ion was used for the detection of the analyte, generating a sensing strategy with a limit of detection (LOD) of 0.98 mu mol L-1. Furthermore, the interaction between the Co2+ ion with the CQDs resulted in the color change of the solution from colorless to pale yellow. Thus, a colorimetric Co2+ sensor was also developed, since there was an absorption band at 315 nm attributed to the formation of the complex CQD + Co2+. The colorimetric method showed an excellent sensitivity to Co2+, with a LOD of 3.01 mu mol L-1. In addition, Principal Component Analysis (PCA) together with Linear Discriminant Analysis (LDA) were used successfully to distinguish different concentrations of Co2+ and different interfering ions present in the solution. Finally, a real sample of blood plasma was properly treated and doped with different concentrations of Co2+, which was successfully quantified via fluorescent method. Therefore, the CQDs obtained in this work are a powerful and versatile Co2+ detection tool.

DYES AND PIGMENTS 215, 111253, 2023. DOI: 10.1016/j.dyepig.2023.111253

[P059-2023] "Diagnostic reference level quantities for adult chest and abdomen-pelvis CT examinations: correlation with organ doses"

Costa, P. R.; **Tomal, A.***; Castro, J. C. D. de; Nunes, I. P. F.; Nersissian, D. Y.; Sawamura, M. V. Y.; Leao, H.; Lee, C.

ObjectivesTo evaluate correlations between DRL quantities (DRLq) stratified into patient size groups for non-contrast chest and abdomen-pelvis CT examinations in adult patients and the corresponding organ doses.MethodsThis study presents correlations between DRLq (CTDIvol, DLP and SSDE) stratified into patient size ranges and corresponding organ doses shared in four groups: inside, peripheral, distributed and outside. The demographic, technical and dosimetric parameters were used to identify the influence of these quantities in organ doses. A robust statistical method was implemented in order to establish these correlations and its statistical significance.ResultsMedian values of the grouped organ doses are presented according to the effective diameter ranges. Organ doses in the regions inside the imaged area are higher than the organ doses in peripheral, distributed and outside regions, excepted to the peripheral doses associated with chest examinations. Different levels of statistical significance between organ doses and the DRLq were presented.ConclusionsCorrelations between DRLq and target-organ doses associated with clinical practice can support guidance's to the establishment of optimization criteria. SSDE demonstrated to be significant in the evaluation of organ doses is also highlighted. The proposed model allows the design of optimization actions with specific risk-reduction results.

INSIGHTS INTO IMAGING 14[1], 60, 2023. DOI: 10.1186/s13244-023-01403-y

[P060-2023] "Displacement sensor based on a large-core hollow fiber and specklegram analysis"

Osorio, J. H.*; Cabral, T. D.*; Fujiwara, E.; Franco, M. A. R.; Amrani, F.; Delahaye, F.; Gerome, F.; Benabid, F.; **Cordeiro, C. M. B.***

The research enterprise towards achieving high-performance hollow-core photonic crystal fibers has led to impressive advancements in the latest years. Indeed, using this family of fibers becomes nowadays an over-arching strategy for building a multitude of optical systems ranging from beam delivery devices to optical sources and sensors. In most applications, an effective single-mode operation is desired and, as such, the fiber micro-structure or the light launching setups are typically designed for achieving such a behavior. Alternatively, one can identify the use of large-core multimode hollow-core fibers as a promising avenue for the development of new photonic devices. Thus, in this manuscript, we propose and demonstrate the utilization of a large-core tubular-lattice fiber for accomplishing a speckle-based displacement sensor, which has been built up by insert-ing and suitably dislocating a single-mode fiber inside the void core of the hollow fiber. The work reported herein encompasses both simulation and experimental studies on the evolution of the multimode intensity distributions within the device as well as the demonstration of a displacement sensor with an estimated resolution of 0.7 mu m. We understand that this investigation identifies a new opportunity for the employment of large-core hollow fibers within the sensing framework hence widening the gamut of applications of this family of fibers.

OPTICAL FIBER TECHNOLOGY 78, 103335, 2023. DOI: 10.1016/j.yofte.2023.103335

[P061-2023] "Electro-Oxidation of Polyols on Bi-Modified Pt in Acidic Media (HCl (TM) O-4). Understanding Activity and Selectivity Trends"

Soffiati, G.; Yukuhiro, V. Y.; Raju, S. P.; Souza, M. B. C. de; Marquezini, L.; **Silva, E. Z. da***; Fernandez, P. S.; San-Miguel, M. A.

Herein we show that Pt(111) and Pt(100) can produce the ketone through the oxidation of the secondary carbon of the polyols. After the Bi modification, the selectivity for the ketone formation increases. On the other hand, we observe that pure and Bi-modified Pt(110) only produced the C3 molecules oxidized in the primary carbon, and it is the only facet that shows an enhancement in the activity due to the modification. In line with these findings, small Pt nanoparticles are not selective for ketone formation. Finally, based on data obtained through DFT calculations, we suggest that positively charged Bi adatoms interact with the OH- groups of the enediol-like intermediate (believed to be the precursor for the ketone/aldehyde production), facilitating the oxidation of the secondary carbon to produce DHA.

CHEMCATCHEM, 2023. DOI: 10.1002/cctc.202300252 Primeira data de acesso: APR 2023

[P062-2023] "Energy harvesting from radio waves using few-layer 2D galena (galenene)"

Karthik, R.; Singh, A. K.; Sreeram, P. R.; Mahapatra, P. L.; **Galvao, D. S.***; Tiwary, C. S.

Radiofrequency (RF) energy harvesting is receiving increased attention in today's digital era due to its potential to replace or improve the longevity of energy storage devices in low-power IoT devices. RF energy is available in the ambient environment, but efficient devices are still not commonly known for RF energy harvesting applications. Here, the main goal is to develop an RF energy harvesting device using multi-layered two-dimensional (2D) galena (PbS). A Schottky diode is fabricated by using 2D galena. RF energy harvesting is demonstrated using a handheld radio transceiver with a carrier frequency of 140-170 MHz. The device extracts RF energy and produces an output DC voltage of a maximum of 1.8 volts and a corresponding output power of 38 mW at 150 MHz, and lights up an LED within a range of 100 cm. At 150 MHz, the device's power conversion efficiency is found to be 19%. DFT calculations support the experimental observations of energy harvesting using 2D galena. The performance results show that 2D galena is a promising material for RF energy harvesting devices.

NANOSCALE 15[20], 9022-9030, 2023. DOI: 10.1039/d3nr00740e

[P063-2023] "Fully atomistic molecular dynamics investigation of the simplest model of dry-draw fabrication of carbon nanotube fibers"

Thomazini, L. F. V.*; Fonseca, A. F.*

Macroscopic assemblies of carbon nanotubes (CNTs) are desirable materials because of the excellent CNT properties. Among the methods of production of these CNT materials, the dry-draw fabrication where CNT fibers (CNTFs) are directly pulled out from a CNT forest is known to provide good physical properties. Although it is known that vertical alignment of CNT bundles within the CNT forest is important, the mechanisms behind the dry-draw fabrication of CNTFs are still not completely understood. The simplest known dry-draw model consists of CNT bundles laterally interacting by only van der Waals forces (vdWf). Here, by fully atomistic classical molecular dynamics simulations, we show that the simplest dry-draw model does not produce CNTFs. We also show one important condition for a pair of adjacent CNT bundles to connect themselves under vdWf only and discuss why it leads to the failure of the simplest model.

MRS ADVANCES, 2023. DOI: 10.1557/s43580-023-00552-y, 2023. Primeira data de acesso: MAR 2023

[P064-2023] "Generalized frustration in the multidimensional Kuramoto model"

Aguiar, M. A. M. de*

The Kuramoto model describes how coupled oscillators synchronize their phases as the intensity of the coupling increases past a threshold. The model was recently extended by reinterpreting the oscillators as particles moving on the surface of unit spheres in a D-dimensional space. Each particle is then represented by a D-dimensional unit vector; for D = 2 the particles move on the unit circle and the vectors can be described by a single phase, recovering the original Kuramoto model. This multidimensional description can be further extended by promoting the coupling constant between the particles to a matrix K that acts on the unit vectors. As the coupling matrix changes the direction of the vectors, it can be interpreted as a generalized frustration that tends to hinder synchronization. In a recent paper we studied in detail the role of the coupling matrix for D = 2. Here we extend this analysis to arbitrary dimensions. We show that, for identical particles, when the natural frequencies are set to zero, the system converges either to a stationary synchronized state, given by one of the real eigenvectors of K, or to an effective two-dimensional rotation, defined by one of the complex eigenvectors of K. The stability of these states depends on the set eigenvalues and eigenvectors of the coupling matrix, which controls the asymptotic behavior of the system, and therefore, can be used to manipulate these states. When the natural frequencies are not zero, synchronization depends on whether D is even or odd. In even dimensions the transition to synchronization is continuous and rotating states are replaced by active states, where the module of the order parameter oscillates while it rotates. If D is odd the phase transition is discontinuous and active states can be suppressed for some distributions of natural frequencies.

PHYSICAL REVIEW E 107[4], 044205, 2023. DOI: 10.1103/PhysRevE.107.044205

[P065-2023] "Graphene as an inhomogeneously broadened two-level saturable absorber"

Goncalves, E. S.*; Fragnito, H. L.*

We show that the inter-band optical conductivity of graphene follows a dependence on intensity that is characteristic of inhomogeneously broadened saturable absorbers, and we obtain a simple formula for the saturation intensity. We compare our results with those from more exact numerical calculations and selected sets of experimental data, and obtain good agreement for photon energies much larger than twice the chemical potential.

APPLIED OPTICS 62[8], C99-C105, 2023. DOI: 10.1364/AO.477430

[P066-2023] "Graphene Nano-Optics in the Terahertz Gap"

Feres, F. H.*; Barcelos, I. D.; Cadore, A. R.; Wehmeier, L.; Norenberg, T.; **Mayer, R. A.***; Freitas, R. O.; Eng, L. M.; Kehr, S. C.; **Maia, F. C. B.***

Graphene nano-optics at terahertz (THz) frequencies (nu) is theoretically anticipated to feature extraordinary effects. However, interrogating such phenomena is nontrivial, since the atomically thin graphene dimensionally mismatches the THz radiation wavelength reaching hundreds of micrometers. Greater challenges happen in the THz gap (0.1-10 THz) wherein light sources are scarce. To surpass these barriers, we use a nanoscope illuminated by a highly brilliant and tunable free-electron laser to image the graphene nano-optical response from 1.5 to 6.0 THz. For nu < 2 THz, we observe a metal-like behavior of graphene, which screens optical fields akin to noble metals, since this excitation range approaches its charge relaxation frequency. At 3.8 THz, plasmonic resonances cause a field-enhancement effect (FEE) that improves the graphene imaging power. Moreover, we show that the metallic behavior and the FEE are tunable upon electrical doping, thus providing further control of these graphene nano-optical properties in the THz gap.

NANO LETTERS 23[9], 3913-3920, 2023. DOI: 10.1021/acs.nanolett.3c00578

[P067-2023] "Graphene woven fabric-polydimethylsiloxane piezoresistive films for smart multi-stimuli responses"

Tung, T. T.; Tran, M. T.; Pereira, A. L. C.; **Cordeiro, C. M. B.***; Nguyen, D. D.; Tai, N. H.; Tran, V. V.; Hsu, C. C.; Joshi, P.; Yoshimura, M.; Feller, J. F.; Castro, M.; Hassan, K.; Nine, M. J.; Stanley, N.; Losic, D.

The outstanding properties of graphene, including its electromechanical property, could be engineered for wearable electronic sensor platforms. The tubular graphene weaved into a mesh or graphene woven fabrics (GWF) has been reported as one of the most sensitive materials for deformation detection, as well as a promising temperature sensor. Herein, we present the performance of our developed flexible, stretchable, and multiple sensitive sensors fabricated from GWF embedded in polydimethylsiloxane (PDMS) film substrate. The GWF/PDMS sensor shows a pressure sensitivity of 0.0142 kPa-1 in a wide linearity range of 0-20 kPa, an outstanding Gauge factor (GF) of 582 at a strain of 6.2 %, and a very high positive sensitivity of 0.0238 degrees C- 1 in the temperature range of 25-80 degrees C. A practical application as a high sensitivity air pressure sensor able to measure low pressures (in the range of Pa to kPa) was also demonstrated. This sensor platform having desirable performance characteristics is an excellent candidate for wearable devices in the healthcare sector.

COLLOIDS AND SURFACES B-BIOINTERFACES 221, 112940, 2023. DOI: 10.1016/j.colsurfb.2022.112940

[P068-2023] "Head-to-head comparison of [Ga-68]Ga-PSMA-11 and [F-18]FDG PET/CT in multiple myeloma"

Souza, S. P. M.; Frasson, F. C.; **Takahashi, M. E. S.***; Duarte, G. B. O.; Castro, V. P.; Pericole, F. V.; Velloso, L. A.; Souza, C. A. de; Lorand-Metze, I.; Santos, A. O.; Ramos, C. D.

PurposeThe aim of this study was to compare [F-18]FDG and [Ga-68]Ga-PSMA-11 PET/CT image findings in patients with multiple myeloma (MM).MethodsTwenty consecutive patients with symptomatic biopsy-proven MM were submitted to whole body [F-18]FDG and [Ga-68]Ga-PSMA-11 PET/CT with a time interval of 1-8 days between procedures. All lesions were counted and had their maximum SUV (SUVmax) measured. Intra-class correlation (ICC) was used to assess the agreement between [F-18]FDG and [Ga-68]Ga-PSMA-11 PET/CT findings.ResultsA total of 266 lesions were detected in 19/20 patients. [F-18]FDG detected 223/266 (84%) lesions in 17 patients and [Ga-68]Ga--PSMA-11 190/266 (71%) lesions in 19 patients. Both procedures did not identify any active lesion in 1 patient. Forty-three (16%) lesions were detected only by [Ga-68]Ga-PSMA-11 and 76 (29%) only by [F-18]FDG. Both tracers identified 147 (55%) lesions. Intralesional mismatch of FDG-PSMA uptake was identified in 25 of these 147 lesions, found in 8 different patients. Different lesions with uptake of only [F-18]FDG or [Ga-68]Ga-PSMA-11 in the same patient were found in 4 patients. The highest SUVmax of [F-18]FDG and [Ga-68]Ga-PSMA-11 had a median (min--max) SUVmax of 6.5 (2.0-37.8) and 5.5 (1.7-51.3), respectively.

[F-18]FDG and [Ga-68]Ga-PSMA-11 respectively identified 18 and 19 soft tissue lesions. False-positive [F-18]FDG findings had minimal or no uptake of [Ga-68]Ga-PSMA-11. Good reliability (ICC >= 0.75) was found for number of lesions, number of soft tissue lesions and highest SUVmax in each patient.Conclusion[F-18] FDG or [Ga-68]Ga-PSMA-11 alone can detect most MM lesions. Almost half of the lesions take up only one of the tracers, reflecting increased glycolysis or angiogenesis in specific lesions, and suggesting their possible complementary role in MM. The marked [Ga-68]Ga-PSMA-11 uptake in some cases raises the possibility of a theranostic approach in selected patients.

EUROPEAN JOURNAL OF NUCLEAR MEDICINE AND MOLECULAR IMAGING, 2023. DOI: 10.1007/s00259-023-06214-3

[P069-2023] "Heterogeneously integrated III-V-on-Si laser with embedded photonic molecule mirrors"

Rezende, G. F. M. de*; Frateschi, N. C.*; Roelkens, G.

We have designed, fabricated, and characterized a III-V-on--Si laser employing photonic molecule mirrors with high potential for laser tunability and control. Resonant mirrors are realized by tailoring supermodes of coupled microrings. A laser threshold of 40 mA (L-band), series resistance of 10 St, and side mode suppression ratio of 40 dB are demonstrated.

JOURNAL OF THE OPTICAL SOCIETY OF AMERICA B-OPTICAL PHYSICS 40[5], 999-1004, 2023. DOI: 10.1364/JOSAB.482670

[P070-2023] "Impact of fibroglandular tissue distribution and breast shape in voxelized breast models for dosimetry in mammography"

Ferrauche, G.*; Tramontin, G.*; Massera, R. T.*; Tomal, A.*

Objective. This work proposes to study the impact of different voxelized heterogeneous breast models (gaussian centered - Gauss(C); gaussian lower - Gauss(L); and fitted equation patient-based on 3D realistic distribution (Fedon et al 2021) - Fit(PB)) for dosimetry in mammography compared to a well--established homogeneous approximation. Influence of breast outer shape also was investigated by comparing semicylindric and anthropomorphic breasts. Approach. By using the PENELOPE (v. 2018) + penEasy (v. 2020) MC code, simulations were performed to evaluate the normalized glandular dose (DgN) and the glandular depth dose (GDD(z)) for different breast characteristics and x-ray beam spectra. Main results. The average DgN overestimation caused by homogeneous tissue approximation was 33.0%, with the highest values attributed to Gauss(L) and Fit(PB) models, where fibroglandular tissue is concentrated deeper in the breast. The observed variation between anthropomorphic and semicylindrical breast shapes was, on average, 5.6%, legitimizing the latter approximation for breast dosimetry. Thicker breasts and lower energy beams resulted in larger overestimation caused by the homogeneous approach, while variations in DgN values among different heterogeneous models were higher for thinner breast and lower energy beams. Moreover, the depth where differences between GDD(z) for different breast models became maximum depends on the axial variation of fibroglandular tissue concentration between each model. The GDD(z) dependence results in a significant variation of the contribution of each breast depth to mean glandular dose (MGD) among the breast models studied. Significance. Intercomparison between different breast models for dosimetry can be useful for estimating more accurate MGD values for population-based dosimetry, for exploring the use of 1D gaussian distribution for breast dosimetry, and for understanding the dose distributions inside the fibroglandular tissues, which could be a novel source of information for risk estimations.

PHYSICS IN MEDICINE AND BIOLOGY 68[7], 074003, 2023. DOI: 10.1088/1361-6560/acbefd

[P071-2023] "Information causality in multipartite scenarios"

Pollyceno, L.*; Chaves, R.; **Rabelo, R.***

The Bell nonlocality is one of the most intriguing and counterintuitive phenomena displayed by quantum systems. Interestingly, such stronger-than-classical quantum correlations are somehow constrained, and one important question to the foundations of quantum theory is whether there is a physical, operational principle responsible for those constraints. One candidate is the information causality principle, which, in some particular cases, is proven to hold for quantum systems and to be violated by stronger-than-quantum correlations. In multipartite scenarios, though, it is known that the original formulation of the information causality principle fails to detect even extremal stronger-than-quantum correlations, thus suggesting that a genuinely multipartite formulation of the principle is necessary. In this work, we advance towards this goal, reporting a different formu-lation of the information causality principle in multipartite scenarios. By proposing a change of perspective, we obtain multipartite informational inequalities that work as necessary criteria for the principle to hold. We prove that such inequalities hold for all quantum resources and forbid some stronger-than-quantum ones. Finally, we show that our approach can be strengthened if multiple copies of the resource are available, or, counterintuitively, if noisy communication channels are employed.

PHYSICAL REVIEW A 107[4], 042203, 2023. DOI: 10.1103/PhysRevA.107.042203

[P072-2023] "Linear response hydrodynamics of a relativistic dissipative fluid with spin"

Montenegro, D.; **Torrieri, G.***

We formulate a Lagrangian hydrodynamics including shear and bulk viscosity in the presence of spin density, and investigate it using the linear response functional formalism. The result is a careful accounting of all sound and vortex interactions close to local equilibrium. In particular, we demonstrate that the mixing of sound waves and vortices via polarization, first observed in the ideal fluid limit, extends to the shear mode once dissipative effects are included. This provides a realization within Lagrangian hydrodynamics of the symmetric shear polarization contribution recently advocated from transport and Zubarev approaches as well as phenomenological considerations. Once causal relaxational dynamics is included, this effect, seemingly puzzling because it results in a nondissipative coupling between a transient mode to an equilibrium quantity, can be understood as a competition between the Israel-Stewart and the polarization relaxation timescale, and a breakdown of local Markovianity. We close by discussing phenomenological implications of these results.

PHYSICAL REVIEW D 107[7], 076010, 2023. DOI: 10.1103/PhysRevD.107.076010

[P073-2023] "Low Pre-Season Hamstring-to-Quadriceps Strength Ratio Identified in Players Who Further Sustained In-Season Hamstring Strain Injuries: A Retrospective Study from a Brazilian Serie A Team"

Veeck, F.; **Ruas, C. V.*;** Pinto, M. D.; Grazioli, R.; Cardoso, G. P.; Albuquerque, T.; Schipper, L.; Valente, H. G.; Santos, V. H.; Dornelles, M.; Rabaldo, P.; Rocha, C. S.; Baroni, B. M.; Cadore, E. L.; Pinto, R. S.

A common pre-season injury prevention assessment conducted by professional football clubs is the hamstring-to-quadriceps (H:Q) strength ratio calculated by peak torque (PT).

However, it is debatable whether players that present low pre--season H:Q ratios are more susceptible to further sustaining in-season hamstring strain injuries (HSI). Based upon retrospective data from a Brazilian Serie A football squad, a particular season came to our attention as ten out of seventeen (similar to 59%) professional male football players sustained HSI. Therefore, we examined the pre-season H:Q ratios of these players. H:Q conventional (CR) and functional (FR) ratios, and the respective knee extensor/flexor PT from the limbs of players further sustaining in-season HSI (injured players, IP) were compared to the proportional number of dominant/non--dominant limbs from uninjured players (UP) in the squad. FR and CR were similar to 18-22% lower ($p < 0.01$), whereas quadriceps concentric PT was similar to 25% greater for IP than UP ($p = 0.002$). Low scores of FR and CR were correlated ($p < 0.01$) with high levels of quadriceps concentric PT ($r = -0.66$ to -0.77). In conclusion, players who sustained in-season HSI had lower pre-season FR and CR compared to UP, which appears to be associated with higher levels of quadriceps concentric torque than hamstring concentric or eccentric torque.

SPORTS 11[4], 89, 2023. DOI: 10.3390/sports11040089

[P074-2023] "Magnetic reversal stability of spin textures in synthetic antiferromagnetic nanodots"

Batistel, T. M.*; Brandao, J.

In this work, we demonstrate the nucleation and stability of spin textures in synthetic antiferromagnetic (SAF) nanodot--shaped systems. By employing micromagnetic simulations at 300 K and zero-field, we obtain phase diagrams distinguishing antiferromagnetic (AFM) single domain, skyrmion and skyrmionium states, among other relevant spin textures, depending on the magnetic and geometric parameters of the circular disk. Furthermore, we investigate the magnetization reversal stability under out-of-plane magnetic fields, revealing that, only under specific conditions, AFM skyrmionic textures are preserved in the absence of magnetic fields. The conservation of the skyrmionic structures along the hysteresis cycle is directly linked with an energy barrier reduction for the nucleation of the spin textures. Our findings demonstrate a very promising route in stabilizing AFM chiral skyrmionic structures in nanodots, at ambient conditions, which is a step towards their use in future antiferromagnetic devices.

JOURNAL OF MAGNETISM AND MAGNETIC MATERIALS 565, 170220, 2023. DOI: 10.1016/j.jmmm.2022.170220

[P075-2023] "Mechanistic Study of Lithium-Ion Battery Cathode Recycling Using Deep Eutectic Solvents"

Alhashim, S. H.; Bhattacharyya, S.; **Tromer, R.***; Kabbani, A.; Babu, G.; Oliveira, E. F.; **Galvao, D. S.***; Ajayan, P. M.

The colossal increase in the use of Lithium-ion batteries (LiBs) necessitates their efficient recycling to ensure a steady supply of essential cathode materials, e.g., Li, Co, and Ni, as well as to tackle huge bulks of battery waste. Deep Eutectic Solvents (DESs) are green solvents with immense potential in the hydrometallurgical recycling of LiB cathodes, although their leaching mechanism has not been explored. We investigate the leaching mechanism of the different transition metals (TM), e.g., Co, Ni, and Li, from the most abundantly used LiB cathode materials NMC and NCA in an ethylene glycol (EG):choline chloride(ChCl) based DES. Leaching experiments performed by altering different parameters and density functional theory (DFT) calculations imply that EG participates in H-bonding and weakens the metal-oxygen bond of the TMs, whereas Cl- attacks the metal center to form chlorometalate complexes. Li on the other hand is surrounded by Cl- ions and leached in the solution. The increased concentration of ChCl in DES ensures the facile formation of these complexes and enhances leaching.

ACS SUSTAINABLE CHEMISTRY & ENGINEERING 11[18], 6914-6922, 2023. DOI: 10.1021/acssuschemeng.2c06571

[P076-2023] "On the viability of a light scalar spectrum for 3-3-1 models"

Cherchiglia, A. L.*; Peres, O. L. G.*

In this work we study an effective version of the 3-3-1 model, in which the particle content is the same of the 2HDM. We show that the inherited structure from the SU(3)(C) circle times SU(3)(L) circle times U(1)(X) gauge group has a series of consequences, the most relevant one being the prediction of the masses of the neutral scalar to be of the order or lower than the mass of the charged scalar. Given current constraints from collider searches, B-physics, as well as theoretical constraints such as perturbativity of quartic couplings and stability of the scalar potential, we find that the new scalars cannot be lighter than 350 GeV.

JOURNAL OF HIGH ENERGY PHYSICS [4], 17, 2023. DOI: 10.1007/JHEP04(2023)017

[P077-2023] "Optics in South America: introduction"

Wiederhecker, G. S.*; Cavalcanti, S. B.; Fontes, A.; Garcia--Sucerquia, J.; Perez, D.; Vera, E.; Bragas, A.; Matos, C. de; Fainstein, A.; Felinto, D.; Milori, D. M. B. P.; Walborn, S. P.

South American optics research has seen remarkable growth over the past 50 years, with significant contributions in areas such as quantum optics, holography, spectroscopy, nonlinear optics, statistical optics, nanophotonics and integrated photonics. The research has driven economic development in sectors like telecom, biophotonics, biometrics, and agri-sensing. This joint feature issue between JOSA A and JOSA B exhibits cutting-edge optics research from the region, fostering a sense of community and promoting collaboration among researchers.

JOURNAL OF THE OPTICAL SOCIETY OF AMERICA A-OPTICS IMAGE SCIENCE AND VISION 40[4], OSA1-OSA2, 2023. DOI: 10.1364/JOSAA.491677

[P078-2023] "Ordered photonic colloidal suspensions"

Jimenez-Villar, E.*; Martins, W. S.; Wetter, N. U.

Ordered photonic structures (photonic crystals) have seen increasing interest in recent years due to their potential applications, which depend on fabrication technologies suitable for mass production. In this paper, we studied by light diffraction the order in photonic colloidal suspensions composed by core-shell (TiO2@Silica) nanoparticles suspended in ethanol and water solutions. Light diffraction measurements show order in these photonic colloidal suspensions, being stronger in ethanol compared with suspensions in water. Strong and long--range Coulomb interaction explains the order and correlation in the scatterers' (TiO2@Silica) position, which favors significantly the interferentialprocesses as localization of light.

APPLIED OPTICS 62[11], 2707-2710, 2023. DOI: 10.1364/AO.477410

[P079-2023] "Photostability of amine-free CsPbBr3 perovskite nanocrystals under continuous UV illumination"

Bonato, L. G.*; Dal Poggetto, G.; Moral, R. F.; **Vale, B. R. de C.***; Germino, J. C.; Almeida, D. B.; Santiago, P.; Fernandez, P. S.; Tormena, C. F.; **Padilha, L. A.***; Nogueira, A. F.

Despite all the recent progress on understanding the optoelectronic and structural properties of the CsPbX3 perovskite nanocrystals (PNCs), the impact of the ligands on their photostability, under continuous UV light soaking, is still ambiguous. To address this subject, in this work, we have investigated the influence of the organic ligand on the photophysics of PNCs by comparing the emission behaviour of CsPbBr3 PNCs capped with oleate (OA) and oleylphosphate (OPA). Based on our experimental observations, we propose two different mechanisms to explain their photostability under continuous UV illumination. We hypothesize that the UV illumination promotes a reconstruction of the nanocrystals' surface, and this process depends on the equilibrium between desorption and adsorption of the surface ligands. In the case of oleate-capped PNCs, this reconstruction is delayed, and even hampered, due to the steric hindered Pb-oleate that desorbs from the surface. In contrast, for the oleylphosphate-caped PNCs, the detached Pb-oleylphosphate can re-adsorb to the surface soon after it leaves because the steric effects are less critical. The results reported here suggest that alkylphosphate ligands can be used to improve the photostability of colloidal PNCs dispersions, an important step towards applications that require continuous excitation, such as back-illuminated LEDs and solar cells.

JOURNAL OF MATERIALS CHEMISTRY C, 2023. DOI: 10.1039/d2tc04953h Primeira data de acesso: MAR 2023

[P080-2023] "Plasmonic Photocatalysis Driven by Indirect Gold Excitation Via Upconversion Nanoparticle Emission Monitored In Situ by Surface- Enhanced Raman Spectroscopy"

Sousa, G. P.; Barros, A. de; **Shimizu, F. M.***; Sigoli, F. A.; Mazali, I. O.

Lanthanide-doped upconversion nanoparticles (UCNPs) absorb low-energy photons, in the near-infrared region (NIR), and emit high-energy photons, in the visible or ultraviolet region (UV/Vis). The higher energy radiation emissions can be used to promote plasmonic photocatalytic reactions by coupling UCNPs with plasmonic nanoparticles. Thus, in this work, highly crystalline beta- NaYF4:Yb3+,Er3+@NaYF4:Nd3+@NaYF4 UCNPs capped with an amino-modified nanosized silica shell were coupled with Au nanospheres (13 +/- 2 nm). The plasmonic-driven dimerization of 4-aminothiophenol (4-ATP) to 4,4 '-dimercap--toazobenzene (DMAB) was carried out solely by using the UCNP visible emissions to excite the Au nanoparticle localized surface plasmon resonance band. The reaction was monitored in situ through surface-enhanced Raman spectroscopy (SERS) and optimal conditions were achieved in order to eliminate secondary influences during spectra acquisition. The SERS substrates containing either UCNPs@SiO2-NH2/Au or SiO2-NH2/Au nanoparticles were prepared by the drop-cast method in silicon substrates. In the studied reaction conditions, plasmonic photocatalytic activity was observed only in the substrates containing UCNPs and Au nanoparticles. The plasmonicdriven reaction was achieved by UCNPs excitation with a 980 nm laser (25.7 mW), aligned in a Raman spectrometer, only after 5 s of exposition. Interactive document mapping (IDMAP), which is an unsupervised pattern recognition method, was applied to analyze the numerous SERS spectra acquired during the plasmonic photocatalytic measurements. The high values found for the silhouette coefficient (0.88 for the Si_SiO2-NH2/Au and 0.76 for the Si_NYF@SiO2-NH/Au substrate) indicate that strong discrimination among the Raman spectra was achieved. Thus, through IDMAP, it was observed that the SERS spectra obtained for the substrates containing either UCNPs@SiO2-NH2/Au or SiO2-NH2/Au corresponded to spectral features, respectively, from the DMAB product and the 4-ATP reagent, evidencing that, in the optimized reaction conditions, the dimerization occurred only through the interaction of the UCNPs with the Au nanospheres.

ACS APPLIED NANO MATERIALS, 2023. DOI: 10.1021/acsanm.3c00704 Primeira data de acesso: APR 2023

[P081-2023] "Post-2000 nonlinear optical materials and measurements: data tables and best practices"

Vermeulen, N.; Espinosa, D.; Ball, A.; Ballato, J.; Boucaud, P.; Boudebs, G.; Campos, C. L. A., V; Dragic, P.; Gomes, A. S. L.; Huttunen, M. J.; Kinsey, N.; Mildren, R.; Neshev, D.; **Padilha, L. A.*;** Pu, M. H.; Secondo, R.; Tokunaga, E.; Turchinovich, D.; Yan, J. S.; Yvind, K.; Dolgaleva, K.; Van Stryland, E. W.

In its 60 years of existence, the field of nonlinear optics has gained momentum especially over the past two decades thanks to major breakthroughs in material science and technology. In this article, we present a new set of data tables listing nonlinear-optical properties for different material categories as reported in the literature since 2000. The papers included in the data tables are representative experimental works on bulk materials, solvents, 0D-1D-2D materials, metamaterials, fiber waveguiding materials, on-chip waveguiding materials, hybrid waveguiding systems, and materials suitable for nonlinear optics at THz frequencies. In addition to the data tables, we also provide best practices for performing and reporting nonlinear-optical experiments. These best practices underpin the selection process that was used for including papers in the tables. While the tables indeed show strong advancements in the field over the past two decades, we encourage the nonlinear-optics community to implement the identified best practices in future works. This will allow a more adequate comparison, interpretation and use of the published parameters, and as such further stimulate the overall progress in nonlinear-optical science and applications.

JOURNAL OF PHYSICS-PHOTONICS 5[3], 035001, 2023. DOI: 10.1088/2515-7647/ac9e2f

[P082-2023] "Probing putative orbital differentiation effects via Eu2+spin dynamics in Sr1-xEuxFe2As2"

Radaelli, M.*; Piva, M. M.*; Souza, J. C.*; Lesseux, G. G.*; Jesus, C. B. R.*; Tobia, D.*; Urbano, R. R.*; Rosa, P. F. S.; **Pagliuso, P. G.***

In this work, we report x-ray powder diffraction, elemental analysis, electrical resistivity, magnetic suscep-tibility, specific heat, and electron spin resonance (ESR) in single crystals of Sr1-xEuxFe2As2. We observed a breakdown of the previously reported scaling between the Eu2+ Korringa relaxation rate obtained from ESR and the spin density wave temperature evolution for Sr-rich samples. This result suggests a distinct evolution of the orbital differentiation of the Fe 3d bands along the Sr--based series when compared to the Ba counterpart. We argue that this difference is related to a larger splitting between the structural (tetragonal-to-orthorhombic) and the Fe-driven spin density wave transitions induced by Eu doping in this series. In fact, our results indicate that the two transitions follow an opposite x-Eu dependence for Sr-concentrated samples. Our work shows that Sr1-xEuxFe2As2 series and the comparison with their Ba-based counterparts are exciting platforms to be explored for understanding the interplay among orbital differentiation, magnetism, and structural distortions in the iron pnictides.

PHYSICAL REVIEW B 107[13], 134512, 2023. DOI: 10.1103/PhysRevB.107.134512

[P083-2023] "Probing the optical and magnetic modality of multi core-shell Fe3O4@SiO2@beta-NaGdF4:RE3+(RE = Ce, Tb, Dy) nanoparticles"

Shrivastava, N.; Ospina, C.; Jacinto, C.; Menezes, A. S. de; **Muraca, D.***; Javed, Y.; **Knobel, M.***; Luo, Z. P.; Sharma, S. K.

A robust yellowish-green emitting multi core-shell Fe3O4@SiO2@beta-NaGdF4:RE3+ (RE=5% Ce, 5% Tb, x% Dy; x=1, 5 and 10 mol.%) nanoparticles (NPs) containing both magnetic and luminescence modalities, are synthe- sized using simple, fast and efficient microwave-assisted hydrothermal method. The Rietveld analysis of X-ray diffraction and high-resolution transmission electron microscopy provides an average crystallite size of-30 nm, confirming the successful coating of the beta--NaGdF4 hexagonal phase over Fe3O4. The detailed photoluminescence investigation suggests a down-converting energy transfer process, Ce3+-> Gd3+-> Tb3+<-> Dy3+ in which Gd3+ ions play a significant intermediate role assisted by Tb3+. The excitation spectra consist of dominant broadband at-252 nm due to Ce3+ (4f-5d), two sharp lines at - 271 nm, and-311 due to Gd3+ (8S7/2 -> 6IJ and 6PJ), and frail f-f transitions due to Tb3+ and Dy3+ ions. The excitation at-252 nm fetches weak and sharp emission of Gd3+ ions at 310 nm, weak broad emission of Ce3+ (300-400 nm), and strong emission color lines of RE3+ (400-700 nm) due to characteristic transitions of Tb3+ (5D4 -> 7FJ, J=6-3), and Dy3+ (4F9/2-6H15/2, 6H13/2), respectively. The quenching phenomenon is observed due to concentration, and back transfer energy is proposed. The mag- netic hysteresis loops display superparamagnetic behavior at 300 K and ferromagnetic ordering at 2 K with a remarkable difference in their magnetization values and confirming the blocking temperatures around physio- logical temperature ranges. The magneto-luminescence characteristics of the bifunctional system can be easily manipulated under an external magnetic field and suggest an efficient candidate for hybrid medical imaging such as MRI plus X-ray imaging and radiation detection.

OPTICAL MATERIALS 137, 113585, 2023. DOI: 10.1016/j.optmat.2023.113585

[P084-2023] "Properties of fermionic systems with the path-integral ground state method"

Ujevic, S.; Zampronio, V.; Abreu, B. R. de; **Vitiello, S. A.***

We investigate strongly correlated many-body systems composed of bosons and fermions with a fully quantum treatment using the path-integral ground state method, PIGS. To account for the Fermi-Dirac statistics, we implement the fixed-node approximation into PIGS, which we then call FN-PIGS. In great detail, we discuss the pair density matrices we use to construct the full density operator in coordinate representation, a vital ingre-dient of the method. We consider the harmonic oscillator as a proof-of-concept and, as a platform representing quantum many-body systems, we explore helium atoms. Pure 4He systems demonstrate most of the features of the method. Complementarily, for pure 3He, the fixed-node approximation resolves the ubiquitous sign problem stemming from anti-symmetric wave functions. Finally, we investigate 3He-4He mixtures, demonstrating the method's robustness. One of the main features of FN-PIGS is its ability to estimate any property at temperature T = 0 without any additional bias apart from the FN ap-proximation; biases from long simulations are also excluded. In particular, we calculate the correlation function of pairs of equal and opposite spins and precise values of the 3He kinetic energy in the mixture.

SCIPOST PHYSICS CORE 6[2], 031, 2023. DOI: 10.21468/SciPostPhysCore.6.2.031

[P085-2023] "Resonant Auger spectroscopy on solid xenon on gold, silver, and copper substrates"

Johansson, F. O. L.; Berggren, E.; **Cornetta, L. M.***; Ceolin, D.; Fondell, M.; Agren, H.; Lindblad, A.

An investigation of the radiationless decay of core excited Xe atoms in the region of Xe L3M4,5M4,5 Auger electron kinetic energies (using x-ray energies in the vicinity of the L3 threshold) is presented for Xe adsorbed on Cu, Ag, and Au. The intensity distribution of the decay channels is different compared with Xe in the gas phase. Charge transfer of the core excited electron occurs within tens of attoseconds in all systems for excitation energies approaching the ionization threshold of the condensed system, whereas charge transfer times are substrate-dependent for lower excitation energies. The determination of partial yields into the decay channels allows for the observation of a decay channel present in the Xe/Cu and Xe/Ag systems but not in the case of Xe/Au. Theoretical calculations allow us to interpret this difference as emanating from varying amounts of the ground state hybridization between Xe and the substrates, which impacts the energy of the Auger final states enabling identification of these states giving rise to system specific features in the experimental data.

PHYSICAL REVIEW A 107[3], 032802, 2023. DOI: 10.1103/PhysRevA.107.032802

[P086-2023] "Robin boundary conditions in acoustic BTZ black holes"

Oliveira, C. C. de*; Mosna, R. A.; Pitelli, J. P. M.

We introduce an analog model for the conformally coupled scalar field on the BTZ black hole. The model is based on the propagation of acoustic waves in a Laval nozzle. Since the BTZ black hole is not a globally hyperbolic spacetime, the dynamics of the scalar field is not well defined until extra boundary conditions are prescribed at its spatial infinity. We show that quasinormal modes (QNMs) satisfying Dirichlet, Neumann, and Robin boundary conditions in the BTZ black hole can be interpreted in terms of ordinary QNMs defined with respect to an appropriately extended nozzle. We also discuss the stability of our model with respect to small perturbations.

PHYSICAL REVIEW D 107[6], 064018, 2023. DOI: 10.1103/PhysRevD.107.064018

[P087-2023] "Schwinger mechanism for gluons from lattice QCD"

Aguilar, A. C.*; Soto, F. de; Ferreira, M. N.; Papavassiliou, J.; Pinto-Gomez, F.; Roberts, C. D.; Rodriguez-Quintero, J.

Continuum and lattice analyses have revealed the existence of a mass-scale in the gluon two-point Schwinger function. It has long been conjectured that this expresses the action of a Schwinger mechanism for gauge boson mass generation in quantum chromodynamics (QCD). For such to be true, it is necessary and sufficient that a dynamically-generated, massless, colour-carrying, scalar gluon+gluon correlation emerges as a feature of the dressed three-gluon vertex. Working with results on elementary Schwinger functions obtained via the numerical simulation of lattice-regularised QCD, we establish with an extremely high level of confidence that just such a feature appears; hence, confirm the conjectured origin of the gluon mass scale. (c) 2023 The Author(s). Published by Elsevier B.V. This is an open access article under the CC BY license (http://creativecommons .org /licenses /by /4 .0/). Funded by SCOAP3.

PHYSICS LETTERS B 841, 137906, 2023. DOI: 10.1016/j.physletb.2023.1379060370-2693

[P088-2023] "Step towards a consistent treatment of chiral theories at higher loop order: the abelian case"

Cherchiglia, A.*

As recently pointed out, regularization schemes defined in four--dimensions may also face inconsistencies in the presence of chiral fermions. In this work, we extend this analysis to two-loop order. Adopting the implicit regularization as working arena, we discuss in detail how a consistent version of the method can be envisaged, and present many of the subtleties that appear at two-loop order using an abelian chiral model as working example. (c) 2023 The Author(s). Published by Elsevier B.V. This is an open access article under the CC BY license (http://creativecommons .org /licenses /by /4 .0/). Funded by SCOAP3.

NUCLEAR PHYSICS B 987, 116104, 2023. DOI: 10.1016/j.nuclphysb.2023.116104

[P089-2023] "Synthesis of two-dimensional van der waals superlattices, heterostructures, and alloys from conversion of sequentially layered sub-nanometer metal films"

Motala, M. J.; Zhang, X.; Kumar, P.; **Oliveira, E. F.***; Benton, A.; Miesle, P.; Rao, R.; Stevenson, P. R.; Moore, D.; Alfieri, A.; Lynch, J.; Austin, D.; Post, S.; Gao, G.; Ma, S.; Zhu, H.; Wang, Z.; Petrov, I.; Stach, E. A.; Kennedy, W. J.; Vangala, S.; Tour, J. M.; **Galvao, D. S.***; Jariwala, D.; Muratore, C.; Snure, M.; Ajayan, P. M.; Glavin, N. R.

Manipulation of bulk material properties by controlling layer--by-layer chemistry and structure of nanomaterials has remained an overarching goal of nanoscience and nanoengineering. In the case of two-dimensional (2D) materials, heterostructures consisting of different compositions, stacking, and orientation can serve as a platform for designing bulk material properties; however, fundamental challenges associated with materials processes have limited material quality and impeded scalability. Most attempts to overcome this limitation have relied on slow layer-by-layer growth or meticulous transfer of grown single layers. Our work describes a method to directly convert easily fabricated sub-nanometer metal multilayer heterostructures on both sapphire and SiO2 substrates followed by con-version to 2D van der Waals superlattices, heterostructures, and alloys. These materials exhibit novel bulk properties compared to individual 2D layers themselves including reduced bandgap, enhanced light-matter coupling, and improved catalytic performance. The process versatility enables tunable orientation, layer structure, and chemistry in an exciting class of 2D nanomaterials and provides an opportunity to generate a wide range of artificially stacked multicompositional 2D structures with controlled morphologies.

MATERIALS TODAY NANO 22, 100319, 2023. DOI: 10.1016/j.mtnano.2023.100319

[P090-2023] "Tailoring radiation pressure on infinite slab using pair of non-collinear plane waves"

Ali, R.*; Dutra, R. S.; Iqbal, S.

The electromagnetic field exerts radiation pressure on the matter and tends to move it either in the backward or forward direction due to net optical pulling or pushing force, respectively. In this work, we reveal an interesting phenomenon of local positive and negative radiation pressure on a dielectric (chiral) slab by using two linearly (circularly) polarized plane waves. In this regard, we develop for the first time, a theory to describe the local radiation pressure appearing due to the interference between the two obliquely impinging (non-collinear) light sources. Under this situation, the radiation pressure strongly depends on the angle of incidence, the polarization of the electromagnetic field and the chirality parameters of the slab (in the case of chiral medium). Our numerical analysis shows that the radiation pressure, exerted on a dielectric or a chiral slab due to the two incident plane waves, is constant over the slab for normal incidence, and it varies locally for an oblique incidence, which indeed follows the conservation laws at all incident angles. It is expected that the results may find fruitful applications in the optical manipulation of soft matter, for instance, cell membranes, chiral surfaces and other soft materials.

OPTICAL MATERIALS 138, 113639, 2023. DOI: 10.1016/j.optmat.2023.113639

[P091-2023] "Testing non-standard neutrino interactions in (anti)-electron neutrino disappearance experiments"

Chaves, M. E.*; Holanda, P. C. de*; Peres, O. L. G.*

We search for scalar and tensor non-standard interactions using (anti)-electron neutrino disappearance in oscillation data. We found a slight preference for non-zero CP violation, coming from both tensor and scalar interactions. The preference for CP violation is led by Daya Bay low-energy data with a significance that reaches similar to 1.7 sigma in the global analysis (and similar to 2.1 sigma when considering only medium baseline reactors data) compared to the standard neutrino oscillation scenario. In some cases, our results indicate that the atmospheric mass squared difference falls outside the range allowed by accelerator long baseline experiments. This suggests the need for further investigation in future work.

JOURNAL OF HIGH ENERGY PHYSICS [3], 180, 2023. DOI: 10.1007/JHEP03(2023)180

[P092-2023]"Tetra-penta-deca-hexagonal-graphene (TPDH--graphene) hydrogenation patterns: dynamics and electronic structure"

Oliveira, C. C.; Medina, M.; **Galvao, D. S.***; Autreto, P. A. S.

The advent of graphene has renewed the interest in other 2D carbon-based materials. In particular, new structures have been proposed by combining hexagonal and other carbon rings in different ways. Recently, Bhattacharya and Jana have proposed a new carbon allotrope, composed of different polygonal carbon rings containing 4, 5, 6, and 10 atoms, named tetra-penta-deca-hexagonal-graphene (TPDH-graphene). This unusual topology results in interesting mechanical, electronic, and optical properties with several potential applications, including UV protection. Like other 2D carbon structures, chemical functionalizations can be used to tune TPDH-graphene's physical/chemical properties. In this work, we investigate the hydrogenation dynamics of TPDH-graphene and its effects on its electronic structure, combining DFT and fully atomistic reactive molecular dynamics simulations. Our results show that H atoms are mainly incorporated on tetragonal ring sites (up to 80% at 300 K), leading to the appearance of well-delimited pentagonal carbon stripes. The electronic structure of the hydrogenated structures shows the formation of narrow bandgaps with the presence of Dirac cone-like structures, indicative of anisotropic transport properties.

PHYSICAL CHEMISTRY CHEMICAL PHYSICS 25[18], 13088-13093, 2023. DOI: 10.1039/d3cp00186e

[P093-2023] "Thickness determination of multiphase layer via combined Rietveld and Grazing Incidence X-ray diffraction approach"

Amorim, V. S. O.; **Calligaris, G. A.*; Cardoso, L. P.*;** Paesano, A.; Valenca, G. P.

Plates of Maraging-300 steel with a chemically grown layer on the surface were prepared by heat treatment in superheated steam at different times. The grown coating on the martensitic substrate was characterized in terms of thickness, compositional and structural information by means of optical and scanning electron microscopies and by Grazing Incidence X-ray Diffraction (GIXRD). The results showed the presence of the hematite, magnetite, and austenite crystalline phases in two different sublayers composing the entire reacted layer: an austenite sublayer over the maraging substrate, and an oxide sublayer at the top, right above the austenite layer, composed of interspersed hematite and magnetite. Quantitative Phase Analysis by the Rietveld method under GIXRD was used to obtain the thicknesses of multiphase chemically reacted layers. The methodology and mathematical formalism are described. The comparison with estimated values from optical and scanning electron microscopy have shown a good agreement between the imaging and diffraction techniques, suggesting that the reacted layer increases progressively with the heat treatment time.

THIN SOLID FILMS 770, 139756, 2023. DOI: 10.1016/j.tsf.2023.139756

[P094-2023] "Time-Dependent Density-Functional Theory for Determining the Electron-Capture Cross Section for Protons Impacting on Atoms and Molecules"

Faria, J. C. de*; Santiago, J.*; Francis, Z.; **Bernal, M. A.***

The use of the Time-Dependent Density-Functional Theory (TDDFT) has increased in the atomic collision field. Calculating the electron-capture cross section (ECCS) for protons is an important question in hadrontherapy and plasma physics, among other areas. In previous studies, it was shown that the approach based on the Local Density Approximation (LDA) fails in the 1-50 keV region, requiring the use of the Optimized Effective Potential (OEP) method. In this work, the ECCS values for 1-50 keV protons impacting on isolated hydrogen, carbon, nitrogen, oxygen, and nitrogenous atoms were determined using the TDDFT. It is shown that adding the Self Interaction Correction to the LDA (LDA-Sic) allows obtaining results close to those provided by the OEP and experiments, with the advantage that the LDA-Sic consumes less computational time. In addition, it was demonstrated that it is imperative to include the spin correction for the specific helium and oxygen cases, in order to get good results for the ECCS using the TDDFT. Theoretical results obtained in this work show excellent agreement with experimental values.

JOURNAL OF PHYSICAL CHEMISTRY A 127[11], 2453-2459, 2023. DOI: 10.1021/acs.jpca.2c08213

[P095-2023] "Transient photocapacitance spectroscopy on Au/TiO2 Schottky diodes with rolled-up nanomembrane electrodes"

Berg, L.; Schnorr, L.; **Merces, L.***; Bettini, J.; Bof Bufon, C. C.; Heinzel, T.

Au / TiO2 Schottky diodes suitable for deep level transient photocapacitance spectroscopy. It is demonstrated that both the binding energy and the capture cross section of the oxygen vacancy can be extracted from the photocapacitance transients using a rate equation model. The values are consistent with those obtained from conventional deep level transient spectroscopy, taken from the same sample. Furthermore, information about the capture process can be extracted.

JOURNAL OF APPLIED PHYSICS 133[6], 065704, 2023. DOI: 10.1063/5.0132445

[P096-2023] "Two coupled qubits under the influence of a minimal, phase-sensitive environment"

Decordi, G. L.; **Vidiella-Barranco, A.***

In this work, we investigate the influence of a minimal, phase--sensitive environment on a system of two coupled qubits. The environment is constituted by a single-mode field initially prepared in a type of Schrodinger cat state, a quantum superposition of two squeezed coherent states. We present an analytical solution to the model and investigate the degradation of the quantum features of the system due to the action of the environment. In particular, we find that the time-averaged linear entropy for long times, (S) over bar (T), has approximately a linear dependence on Mandel's Q parameter as well as on the variance of the (X) over cap quadrature of the initial state of the environment.

PHYSICS LETTERS A 468, 128750, 2023. DOI: 10.1016/j.physleta.2023.128750

[P097-2023] "Prehydrodynamic evolution in large and small systems"

Silva, T. N. da; **Chinellato, D. D.*; Giannini, A. V.*; Takahashi, J.***; Ferreira, M. N.; Denicol, G. S.; Hippert, M.; Noronha, J.; Luzum, M.

We extend our previous investigation of the effects of prehydrodynamic evolution on final-state observables in heavy-ion collisions [38] to smaller systems. We use a state-of-the-art hybrid model for the numerical simulations with optimal parameters obtained from a previous Bayesian study. By studying p-Pb collisions, we find that the effects due to the assumption of a conformal evolution in the prehydrodynamical stage are even more important in small systems. We also show that this effect depends on the time duration of the pre-equilibrium stage, which is further enhanced in small systems. Finally, we show that the recent proposal of a free-streaming with subluminal velocity for the pre-equilibrium stage, thus effectively breaking conformal invariance, can alleviate the contamination of final-state observables. Our study further reinforces the need for moving beyond conformal approaches in pre-equilibrium dynamics modeling, especially when extracting transport coefficients from hybrid models in the high-precision era of heavy-ion collisions.

PHYSICAL REVIEW C 107[4], 044901, 2023. DOI: 10.1103/PhysRevC.107.044901

[P098-2023] "Ultrashort pulse generation in erbium-doped fiber lasers in South America: a historical review"

Souza, E. A. T. de; Steinberg, D.; Saito, L. A. M.; Rosa, H. G.; Zapata, J. D.; Matos, C. J. S. de; **Fragnito, H. L.*; Cruz, C. H. B.***

This paper reviews the scientific contributions of the last 30 years on erbium-doped fiber laser ultrashort pulse generation in South America. The focus is on contributions authored in South American institutions. It reveals a wide variety of laser cavities, ranging in length from a few centimeters to tens of kilometers, and optical pulses, from tens of femtoseconds to nanoseconds, with fully controlled average and peak powers. Furthermore, different approaches for ultrashort pulse generation using active (synchronous and asynchronous) and/or passive modelocking techniques are discussed, as well as the employment of nonlinear optical phenomena (Kerr effect) and several two-dimensional nanomaterials as saturable absorbers, such as carbon nanotubes, graphene, graphite, graphene oxide, reduced-graphene oxide, semiconductor transition metal dichalcogenides, and black phosphorus.

Finally, the paper revisits and discusses several advances, important milestones, and records on ultrashort pulse generation in erbium-doped fiber lasers, with many essential outcomes attesting to the high quality of research carried out in South America in the field of ultrafast fiber lasers.

JOURNAL OF THE OPTICAL SOCIETY OF AMERICA B-OPTICAL PHYSICS 40[4], C148-C176, 2023. DOI: 10.1364/JOSAB.482638

[P099-2023] "Utilization of two-dimensional multicomponent Quasicrystal for NO2 gas detection"

Mishra, S. S.; Kumar, S.; Kumbhakar, P.; Katiyar, N. K.; **Tromer, R.***; Woellner, C. F.; **Galvao, D. S.***; Tiwary, C. S.; Kumar, M.; Biswas, K.

The two-dimensional (2D) materials provide an effective ultra--sensitive response for sensing due to the large surface area available for the analyte. Al70Co10Fe5Ni10Cu5 (Quasicrystal--QC) alloy can be effectively exfoliated into a 2D form consisting of the decagonal quasicrystalline phase. The ultrathin thickness of a few nm (similar to 6 nm) was achieved, exhibiting anisotropic electron-transport properties. The 2D-QC shows pseudo-conducting behavior in the planar region, which endowed the material in nanosheets to work as ultrasensitive NO2 gas sensors (1-100 ppm) at 100 degrees C. The fabricated device exhibits a NO2 gas response (Delta R/R-a %) of 46% compared to its bulk counterpart. In addition, the mechanism of gas sensing was further corroborated using density functional theory (DFT) simulations and strongly support the interpretation of the experimental data.

MATERIALS CHEMISTRY AND PHYSICS 298, 127449, 2023. DOI: 10.1016/j.matchemphys.2023.127449

[P100-2023] "Witnessing Nonclassicality in a Causal Structure with Three Observable Variables"

Lauand, P.*; Poderini, D.; Nery, R.; Moreno, G.; **Pollyceno, L.*; Rabelo, R.*;** Chaves, R.

Seen from the modern lens of causal inference, Bell's theorem is nothing other than the proof that a specific classical causal model cannot explain quantum correlations. It is thus natural to move beyond Bell's paradigmatic scenario and consider different causal structures. For the specific case of three observ--able variables, it is known that there are three nontrivial causal networks. Two of those are known to give rise to quantum nonclassicality: the instrumental and the triangle scenarios. Here we analyze the third and remaining one, which we name the Evans scenario, akin to the causal structure underlying the entanglement-swapping experiment. We prove a number of results about this elusive scenario and introduce new and efficient computational tools for its analysis that can also be adapted to deal with more general causal structures. We do not solve its main open problem-whether quantum nonclassical correlations can arise from it-but give a significant step in this direction by proving that postquantum correlations, analogous to the paradigmatic Popescu-Rohrlich box, do violate the constraints imposed by a classical description of the Evans causal structure.

PRX QUANTUM 4[2], 020311, 2023. DOI: 10.1103/PRXQuantum.4.020311

[P101-2023] "Y-Substitution effects in the crystal field of the trigonal YxRE1-xNi3Ga9 (RE = Tb, Dy, and Ho)"

Mendonca, E. C.; Jesus, C. B. R.; Duque, J. G. S.; Garcia, D. J.; Bittar, E. M.; **Souza, J. C.*; Pagliuso, P. G.***

Multipolar ordering arising from the interplay between crystalline electric field (CEF) effects and magnetic interactions has been gaining more attention in 4f systems. In this work, we explore this possibility in the chiral magnets RENi3Ga9 (RE = Tb, Dy and Ho; x = 0.15 and 0.30) through Y-dilution. We present tem-perature-dependence of the M/H curves, isothermal magnetization and heat-capacity experiments. Single crystalline samples grown by Ga self flux allow us to measure the magnetic properties for different crys-tallographic directions. X-ray diffraction patterns analyzed by Rietveld method indicate that all samples crystallize in a trigonal ErNi3Al9-type structure with space group R32. Our results are consistent with an antiferromagnetic order with transition temperatures TN < 20 K for all the studied samples, which decrease gradually with Y-substitution. By using a mean field model including anisotropic near-and next-near-neighbors magnetic interactions and the trigonal CEF Hamiltonian, we are able to study in detail the evolution of the crystal-field scheme and magnetic couplings for these compounds. We show that the spatial charge distribution between the compounds are in agreement, increasing the confidence of the obtained CEF schemes. Finally, we compare our fittings with disorder simulations assuming that CEF effects should not evolve as a function of Y-substitution. Our results show that only disorder effects do not fully describe the experimental data, which may indicate that quadrupolar degrees of freedom indeed have a role in the magnetic properties of this family.

JOURNAL OF ALLOYS AND COMPOUNDS 947, 169459, 2023. DOI: 10.1016/j.jallcom.2023.169459

[P102-2023] "Zn Vacancies as Hydrogen Trap Sites in Polar Surfaces: A New Stabilization Mechanism for the ZnO(0001)-(2?2) Surface Reconstruction"

Lima, L. H. de; Silva, W. S. E.; **Prior, I. A. S.*; Landers, R.*; Siervo, A. de***

The (2x2) reconstruction of the ZnO(0001) surface has been investigated by X-ray photoelectron diffraction (XPD). Comparing the XPD measurements with multiple-scattering simulations, the single Zn vacancy per (2x2) surface unit cell model is confirmed, and structures with O adatoms are ruled out. The analysis indicates an outward relaxation of the topmost Zn layer, in contrast to the usually reported results by density-functional theory (DFT) calculations. On the basis of DFT, we describe a new stabilizing mechanism of the polar ZnO surface through surface reconstruction where the Zn vacancies are occupied by three hydrogens atoms. The DFT surface relaxation of the proposed model is in excellent agreement with the XPD findings. Our DFT simulations also strongly indicate that the migration of hydrogens atoms to the surface, coming from the bulk, may influence the desorption of the surface Zn atom to create the vacancy.

JOURNAL OF PHYSICAL CHEMISTRY C, 2023. DOI: 10.1021/acs.jpcc.3c00567 Primeira data de acesso: APR 2023 **(Artigo destaque de capa)**

***Autores da comunidade IFGW**
Fonte: Web of Science on-line (WOS)

Defesas de Dissertações do IFGW

[D005-2023] "Holografia Celestial a partir do limite de espaço plano de AdS/CFT"
Aluno: Leonardo Pipolo de Gioia
Orientador: Prof. Dr. João Paulo Pitelli Manoel
Data: 12/05/2023

[D006-2023] "Investigating the Performance of Machine Learning Algorithms for Muon Signal Identification at the Pierre Auger Observatory"
Aluno: João Vitor Reginatto Akim
Orientador: Profa. Dra. Carola Dobrigkeit Chinellato
Data: 16/05/2023

[D007-2023] "Inclusão da criação e transporte de portadores de carga em detectores semicondutores no código de simulação Monte Carlo PENELOPE: efeitos na formação da imagem radiográfica"
Aluno: Hítalo Rodrigues Mendes
Orientador: Profa. Dra. Alessandra Tomal
Data: 18/05/2023

[D008-2023] "Application of Arapuca technology for detection of scintillation light in liquid argon and Cherenkov radiation in water"
Aluno: Gabriel Botogoske
Orientador: Profa. Dra. Ana Amélia Bergamini Machado
Data: 19/05/2023

[D009-2023] "Otimização Numérica de Dispositivos Optomecânicos"
Aluno: Gabriel Henrique Martins de Aguiar
Orientador: Prof. Dr. Thiago Pedro Mayer Alegre
Data: 19/06/2023

[D010-2023] "Condutividade Hall térmica em uma fase de sólido de singletos de um antiferromagneto frustrado"
Aluno: Lucas da Silveira Buzo
Orientador: Prof. Dr. Ricardo Luís Doretto
Data: 05/07/2023

Defesas de Teses do IFGW

[T004-2023] "Uso de Dinâmica Molecular Quântica (TDDFT) para Adaptação do Campo de Forças REAXFF para Estudo de Colisões Rápidas de Prótons com Material Orgânico"
Aluno: Jhaison Costa de Faria
Orientador: Prof. Dr. Mario Antonio Bernal Rodriguez
Data: 19/05/2023

[T005-2023] "Investigation of the Electronic Structure of Materials with Complex Topological States by means of Angle Resolved Photoemission Spectroscopy"
Aluno: Kevin Raduenz Pakuszewski
Orientador: Prof. Dr. Eduardo Granado Monteiro
Data: 19/05/2023

[T006-2023] "Laser de III-V-EM-Si Integrado Heterogeneamente com Espelhos Ressonantes à Base de Cavidades Acopladas"
Aluno: Guilherme Fórnias Machado de Rezende
Orientador: Prof. Dr. Newton Cesario Frateschi
Data: 29/05/2023

[T007-2023] "Dinâmica caótica de corpos extensos orbitando buracos negros"
Aluno: Fernanda de Farias Rodrigues
Orientador: Prof. Dr. Ricardo Antonio Mosna
Data: 26/06/2023

[T008-2023] "Deep Learning para Detectar Comunidades de Desinformação por Similaridade Semântica no Twitter"
Aluno: Rafael Geurgas Zavarizz
Orientador: Prof. Dr. Leandro Russovski Tessler
Data: 10/07/2023

Fonte: Portal IFGW/Pós-graduação - Agenda de Colóquios, Defesas e Seminários.
Disponível em: http://portal.ifi.unicamp.br/pos-graduacao

Defesas de Dissertações e Teses do PECIM

[Pe001-2023]"Sobre a propagação de desinformações científicas nas redes sociais: uma pesquisa etnográfica no twitter para reflexões sobre a educação em ciências"
Aluno: Gabriela Fasolo Pívaro
Orientador: Prof. Dr. Gildo Girotto Júnior
Banca: Prof. Dr. Gildo Girotto Júnior - IQ/ UNICAMP, Profa. Dra. Ana de Medeiros Arnt - IB/ UNICAMP, Prof. Dr. Mauricio Compiani - IG/ UNICAMP, Dr. Alexandre Bagdonas - Universidade Federal de Lavras /Lavras, Dra. Sonia Rocio Casillas Martín - Universidad de Salamanca /Salamanca, Dr. Steve da Silva Vicentim - Universidade Federal do Cariri - UFCA /Cariri (suplente), **Prof. Dr. Mauricio Urban Kleinke - IFGW/ UNICAMP (suplente)***, Dr. Diogo Burigo Almeida - Universidade Federal do ABC - Centro de Ciências Naturais e Humanas / São Bernardo do Campo (suplente), Dr. Renato Pacheco Villar - Colégio Bandeirantes - São Paulo /São Paulo (suplente)
Data: 15/06/2023
Exame de Defesa: Doutorado

Fonte: Página do Programa de Pós-Graduação Multiunidades em Ensino de Ciências e Matemática - PECIM
Disponível em: https://www.pecim.unicamp.br/bancas

Abstracta

Instituto de Física
Diretor: Profa. Dra. Mônica Alonso Cotta
Diretora Associada: Prof. Dr. Marcos Cesar de Oliveira
Universidade Estadual de Campinas - UNICAMP
Cidade Universitária Zeferino Vaz
13083-859 - Campinas - SP - Brasil
e-mail: secdir@ifi.unicamp.br
Fone: +55 19 3521-5300

Publicação

Biblioteca do Instituto de Física Gleb Wataghin
http://portal.ifi.unicamp.br/biblioteca
Instagram: @bif.unicamp
Telegram: t.m/bifunicamp

Diretora Técnica: Sandra Maria Carlos Cartaxo
Coordenadora da Comissão de Biblioteca: Profa. Dra. Arlene Cristina Aguilar

Elaboração:
Maria Graciele Trevisan (Bibliotecária)
contato: infobif@ifi.unicamp.br